Mechanistic study on the asymmetric synthesis of the Wieland-Miescher ketone and analogs

Chunhui Liu,[a],[b] Ben Bradshaw,*[c] Feliu Maseras,[a],[d] Josep Bonjoch,[c] and Maria Besora*[a],[e]

Abstract: The organocatalyzed synthesis of the Wieland-Miescher ketone (WMK) via *N*-sulfonyl-binamprolinamide catalysis was investigated using experimental and computational tools. A mechanistic proposal is presented describing the origin of the high enantioselectivity, which rivals that of enzymes/aldolases. The computational study reveals that the role of the prolinamide catalyst is to lower the reaction barrier and determine the stereoselectivity of the product achieved, while the role of the carboxylic acid is to facilitate proton transfer steps. The effect of the acid co-catalyst was confirmed by experiments. The role of the structure of the BINAM backbone and the effect of the sulfonamide group are uncovered experimentally and computationally. Calculations show that a rigid highly defined catalytic pocket due to covalent and steric interactions induces conformational changes in the triketone substrate to maximize interactions.

Introduction

Proline-based organocatalysts are a clear example of the success of organocatalysis. The Hajos–Parrish–Eder–Sauer–Wiechert reaction was the first example of a proline-catalyzed reaction.[1,2] It is an intramolecular aldol reaction that allows access to both the Hajos-Parrish ketone (HPK) and the Wieland-Miescher ketone (WMK),[3] important building blocks for the synthesis of natural products, notably steroids and terpenoids (Scheme 1).The high enantioselectivity of both reactions awoke the interest of researchers in asymmetric organocatalysis and its exploitation led to an improvement of the reactivity, selectivity and substrate scope of organocatalytic reactions,[4] and this global procedure is a very efficient synthetic protocol for the synthesis of ketones WMK.[5,6] Proline organocatalysis has strong similarities with some bio-catalysis, such as that by Type I aldolases.[7] Organocatalysis has some advantages over biocatalysis such as simplicity, relatively straightforward catalyst modification, wide substrate scope and compatibility with organic solvents. However, it also has disadvantages such as (usually) less enantioselectivity. For example, in the proline organocatalyzed synthesis of **2**, the enantioselection of the cyclization step is moderate giving just around 70% enantiomeric excess (ee).[2]

Scheme 1. The Hajos-Parrish-Eder-Sauer-Wiechert reaction, from reference 2.

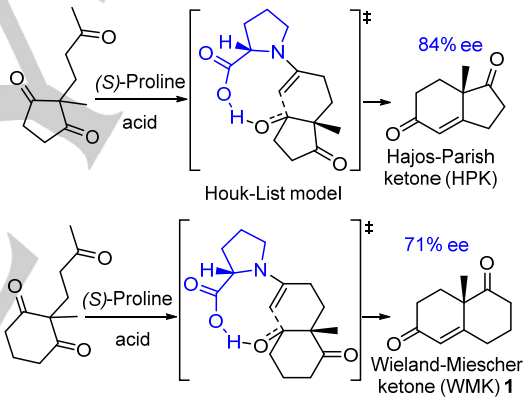

Mechanistic studies on the Hajos–Parrish–Eder–Sauer–Wiechert reaction were essential to understand organocatalysis.[8] The origin of the catalysis was controversial until theoretical and experimental studies were carried out. A mechanism postulating an hemiaminal (carbinolamine) intermediate was early proposed by Hajos.[1] Another mechanism proposed instead the formation of an enamine intermediate with two proline units[9] but was discarded following later experimental studies.[10,11] Bahmanyar and Houk proposed another mechanism where a single proline unit participates forming a hydrogen bond between the proline carboxyl group and the dione.[12] A new enamine mechanism was reported by List, Lerner and Barbas.[13] And later the Houk-List mechanism was postulated based on computational and experimental results involving the formation of an enamine intermediate with a single proline unit.[11] An alternative to the Houk-List model was proposed by Seebach and Eschenmoser.[14] This mechanism proposes that the catalytic cycle goes through the formation of a bicyclic oxazolidinone. This species has been experimentally detected,[15] but some authors proposed that it was just parasitic or at least not involved in the main catalytic

[a] Dr. Chunhui Liu, Dr. Maria Besora, Prof. Feliu Maseras
Institute of Chemical Research of Catalonia (ICIQ), The Barcelona Institute of Science and Technology.
Avgda. Països Catalans, 16, Tarragona 43007
E-mail: maria.besora@urv.cat
[b] Dr. Chunhui Liu
School of Chemistry and Chemical Engineering
Xuchang University of China
No. 88 Bavi Road, Xuchang, Henan, 461000 (P. R. China)
[c] Dr. Ben Bradshaw, Prof. Josep Bonjoch
Laboratori de Química Orgànica, Facultat de Farmàcia, IBUB
Universitat de Barcelona
Avda. Joan XXIII, 27-31 Barcelona 08028
E-mail: ben.bradshaw@ub.edu
[d] Prof. Feliu Maseras
Departament de Química
Universitat Autònoma de Barcelona
[e] Dr. Maria Besora
Departament Química Física i Inorgànica
Universitat Rovira i Virgili (URV)
C/ Marcel.lí Domingo s/n Tarragona 43007

Supporting information for this article is available on WWW under https://doi.org/

cycle,[16,17] whilst others argue that oxazolidinones have in fact a pivotal role in proline catalysis.[14,15,18] Enamine intermediates supporting the Houk-List mechanism have also been detected,[19] and in fact this mechanism has been shown to operate in a number of cases,[17,20] and it is the only one that can operate in our study, as the Seebach-Eschenmoser mechanism requires a base, which is not present in our experimental conditions.

Some of us have previously applied computational tools to determine the origin of the selectivity in cycloaddition reactions catalyzed by phosphoric acid derivatives.[21] We have also previously reported an efficient and highly enantioselective method for the synthesis of **1** and analogs using the N-Ts(S_a)-binam-L-Pro catalyst **3**, under solvent-free conditions.[22] This simple method could be used to prepare large quantities of WMK and analogs with very high enantioselectivity (>94-97%) (Scheme 2) and it remains a very efficient synthetic protocol, even considering other procedures reported later.[5]

Scheme 2. Synthesis of WMK using BINAM-sulfonamide catalyst **3**

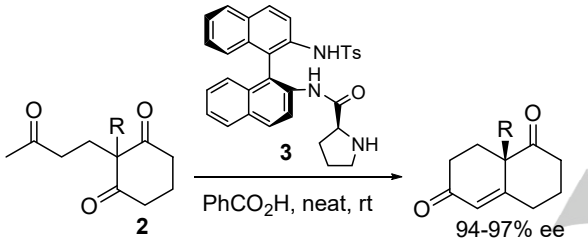

- Very low catalytic loadings
- Very high enantioselectivity
- No work-ups/chromatography required

In this paper, we present a combination of experimental and theoretical studies to elucidate the details of the catalytic mechanism and identify the elements essential for the stereocontrol in the synthesis of Wieland-Miescher ketone using a BINAM-sulfonamide catalyst. Experimentally, different reaction conditions and acids were used to investigate the role of the acid co-catalyst. Organocatalysts with modified structures were also prepared and tested to see the effect of the changes in the enantioselectivity. Computationally the mechanism was studied considering different models. The origin of the near-perfect enantioselectivity was elucidated. The role of the acid co-catalyst was investigated as well as its involvement in the enantiocontrol. The effect of substitutes in the prolinamide catalyst was computationally investigated, and their effect on the enantioselectivity was rationalized.

Results and Discussion

Experimental Synthetic Studies: During the course of our experimental investigations we studied three key variables (a) the catalyst loading, (b) the acid co-catalyst and (c) the catalyst structure. One of the challenges in organocatalysis is to find chiral organocatalysts that are as reactive and stereoselective as some of the best transition-metal catalysts. Unfortunately, in order to attain reasonable reaction rates and stereoselectivity large loadings of the organocatalyst are often required, which often makes it impractical to produce large quantities of material in an economical manner, for example, in total synthesis. Thus, minimizing the quantity of catalyst used whilst maintaining a high ee is an essential goal of organocatalysis. One solution is the design of bifunctional catalysts like **3**, which has a secondary amine group and tunable H-bond donor groups that work cooperatively to bind and activate the reacting groups via pre-organization and stabilization of the transition state of the substrate. This in turn leads to acceleration of the reaction rate and high levels of stereoselectivity. Indeed, as can be seen in Table 1, catalyst **3** can be used in very low quantities with much higher enantioselectivities (entry 1, Table 1) than the corresponding reaction with proline itself (which requires 25% of catalyst and gives only 71% ee).

Table 1. Screening of catalyst and acid concentration (more entries available in the Supporting Information,Table S1).[a]

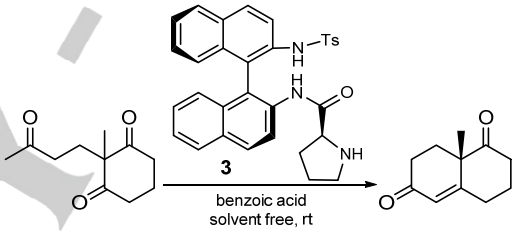

Entry	Catalyst (mol %)	Acid (mol %)	Time/d	Yield[b]	ee[c](%)
1	5	1	1	95	90
2	2.5	1	4	95	92
3	1	1	14	n.d [d]	n.d [d]
4	1	2.5	5-6	97	90
5	2	0.5	7	94	94
6	0.5	2.5	18	98	89

[a] Reactions were performed on a 500 mg scale of triketone **2** (R=Me) with benzoic acid as co-catalyst. [b] Yields of isolated product. [c] Determined by HPLC analysis on a chiral stationary phase. [d] not determined.

Interestingly, it was observed that decreasing the catalyst loading actually improved the enantioselectivity (entry 2, Table 1). It is likely that at higher concentrations the bifunctional nature of the catalyst results in self-aggregation to form distinct catalytic species which negatively affect the enantioselectivity.[23] However, at very low catalytic loadings there was a significant decline in the rate of the reaction (entry 3, Table 1). This could be offset by increasing the quantity of the acid co-catalyst (entry 4, Table 1). However, this resulted in a slight erosion of the enantioselectivity, which we attribute to the additional acid interfering with the H-bonding essential for the bifunctional reactivity of the catalyst.

Further attempts to counterbalance these two opposing factors allowed us to obtain slightly higher enantioselectivities with 2% catalyst and 0.5% acid co-catalyst (entry 5, Table 1), although attempts to find conditions using lower loadings of the catalyst were unfruitful (entry 6, Table 1 and entries 7-11 in the Supporting Information, Table S1).[24] Finally, the conditions of entry 4 were optimal in terms of reaction time, catalyst loading and enantioselectivity. It was therefore with these conditions that we decided to proceed to the screening of alternative acid co-catalysts. It should be noted that applying these same conditions gave no reaction when typical solvents were employed (DMSO, MeCN and i-PrOH), which is likely again due to interference with the hydrogen bonding essential for the bifunctional nature of the catalyst. Notably, the use of a non-hydrogen bonding solvent, dichloromethane, gave some reactivity (64% conversion after 10 days) with a reduced ee (82%).

Table 2. Screening of different acid co-catalysts (more entries available in the Supporting Information, Table S2).[a]

Entry[j]	Acid	pKa	Time/d	Yield [b]	ee% [c]
1	stearic	4.9	5	n.d[d]	n.d[d]
2	acetic	4.76	6-7	92	87
3	benzoic	4.2	5-6	97	90
4	4-chlorobenzoic	4.0	5	91	90
5	formic	3.77	3	97	90
6	L-malic	3.4, 5.13	5	97	88
7	D-malic	3.4, 5.13	5	98	87
8	2-fluorobenzoic	3.27	3	97	90
9	2-nitrobenzoic	2.17	3	95	85
10	trifluoroacetic	0.52	3	n.d[d]	n.d[d]

[a] Reactions were performed on a 500 mg scale of triketone **2** (R=Me) using 1 mol% of catalyst **3** and 2.5 mol% of acid co-catalyst at rt under solvent-free conditions. [b] Yields of isolated product. [c] Determined by HPLC analysis on a chiral stationary phase. [d] not determined

The Houk-List model[11] does not specify the role of the acid co-catalyst, as it may act to form the enamine and eliminate the aldol product or it may be involved in the enantioselective step, as has been observed in other catalytic systems. To determine if the acid co-catalyst plays an important role in the reaction, we screened a significant number of acids covering a wide range of pKa values (see Table 2, or Table S2 Supporting Information for a complete version). Experiments were performed with N-Ts(S_a)-binam-L-prolinamide organocatalyst **3** and the substrate 2-(2-oxopropyl)-2-methyl-cyclohexane-1,3-dione, **1**. We also checked a number of chiral acids to see if they had any effect on the enantioselectivity of the reaction. We observed that: i) at the extremes of the studied pKa range the reaction was inefficient/not effective (entries 1, 2, 9 and 10, Table 2) but the rest the reaction proceeds in an analogous fashion to that of benzoic acid; ii) the use of a chiral acid co-catalyst proved to have no effect (no increased stereoinduction, see entries 6 and 7 Table 2); and iii) we were pleased to observe a significant rate enhancement as the pKa decreased without erosion of the ee (compare entry 3 with entries 4, 5 and 8, Table 2). From this screening test, formic acid presented itself as the best candidate, as its relatively high volatility allowed it to be easily removed at the end of the reaction, outperforming benzoic acid, which sometimes contaminates the final product in large scale reactions.

Figure 1. Screening of the experimentally modified binam-prolinamide catalysts. Yields correspond to isolated product. ee determined by HPLC analysis on a chiral stationary phase.

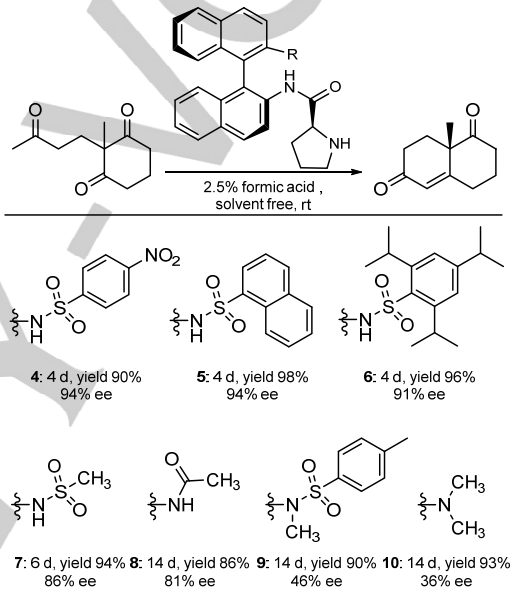

Following this study, the catalyst was modified to investigate the effect of the catalyst structure. A number of BINAM catalysts were synthesized, which included modification of the sulfonamide -NH(Ts) group. By replacing the sulfonamide by other functional groups R, the effect of this group was investigated. The modifications performed are of different types: i) tuning of the electronic and steric properties of the sulfonamide group (catalysts **4**, **5**, **6** and **7**); (ii) replacement of the sulfonamide by an amide (catalyst **8**); and (iii) substitution of a secondary sulfonamide by a tertiary (catalyst **9**, change of the amide hydrogen by a methyl) and use of a dimethylamino group (catalyst **10**). The scheme of the catalysts and the experimental results obtained in terms of yield and enantioselectivity are summarized in Figure 1. The modification of the sulfonamide group had a significant effect on the enantioselectivity. The most interesting result is the effect of aromaticity: increasing the aromatic rings (binapthyl catalyst **5**) led to an increase in 4% ee with respect to tosylamide (catalyst **3**), whereas replacing the aromatic group with a simple methyl group (catalyst **7**) led to a decrease by the same amount. It can also be seen that the hydrogen of the secondary amides is key, as tertiary amides showed a poor enantiomeric performance.

Figure 2. Postulated enamine formation mechanism. Energies correspond to relative free energies in kcal.mol^{-1} with respect to separate reactants. The naphthyl groups of the BINAM catalyst have been substituted by stars for clarity. Forming and breaking bonds in transition states are presented in red.

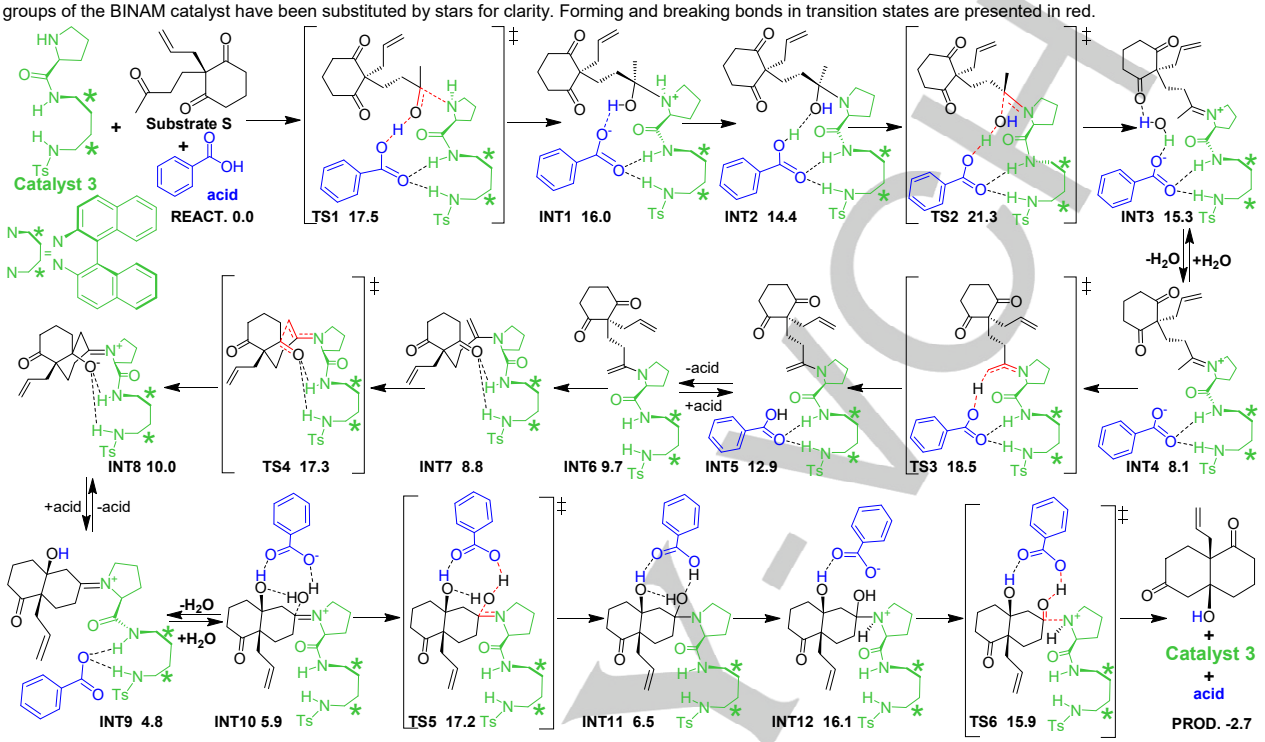

Computational studies of the Reaction Mechanism: Different computational models were built to find out the reaction mechanism in presence and absence of the acid co-catalyst, and multiple mechanistic possibilities were taken into account. Only the preferred ones are summarized in this document. Calculations were carried out with the real N-Ts(S_a)-binam-L-prolinamide organocatalyst **3**, the real substrate **S**, **2** (R=$CH_2CH=CH_2$) = 2-(prop-2-en-1-yl)-2-(2-oxopropyl) cyclohexane-1,3-dione, and benzoic acid as co-catalyst. The dielectric environment was considered through a continuum model.

The results of the mechanistic computational studies carried out considering benzoic acid as co-catalyst led us to propose the mechanism presented in Figure 2. The first step consists of the attack of the prolinamide catalyst **3** to the acyclic carbonyl group of the triketone **S** to form the C-N bond. The process takes place with assistance of benzoic acid (co-catalyst): as the formation of the C-N bond takes place, there is also a proton transfer from benzoic acid to the carbonyl, see **TS1** in Figure 2. Two transition state configurations were located for the C-N bond formation, *trans* being the most stable. Intermediate **INT1** is formed with the new C-N and O-H bonds. In this intermediate the nitrogen of the proline group bears formally a positive charge. Through a process with no barrier in potential energy, the proton on the proline is abstracted by the benzoate anion generated in the same step, resulting in **INT2**. The reaction follows with formation of an iminium cation through **TS2**. The newly formed hydroxyl group (former carbonyl) is protonated by benzoic acid generating a water molecule, and the C-O bond is broken. After the formation of the iminium intermediate **INT3**, the system evolves towards the formation of enamine **INT5**, which is formed through an intramolecular deprotonation process. The co-catalyst then departs the system, resulting in intermediate **INT6**. **INT6** can then rearrange to **INT7**, which is ready to make a C-C bond and close the 6-membered ring in **INT8**. After undergoing by attack of the enamine C=C bond to the carbonyl of the dione the formation of a C-C bond, **TS4** closes the 6-membered cycle generating **INT8**. The co-catalyst then re-enters the system to allow the release of the products and the regeneration of the catalyst. The alternative mechanism that goes from **INT5** to **INT9** with participation of the acid co-catalyst is higher in energy (about 3 kcal/mol). It is presented in detail in the Supporting Information.

The free energies of the transition states for the formation of the carbinolamine, iminium, enamine, bicylic iminium, and bicylic carbinolamine intermediates and products are located at 17.5, 21.3, 18.5, 17.3, 17.2 and 15.9 kcal.mol^{-1} and all intermediates have energies above reactants. Hence the rate-determining step of the reaction is the formation of the first iminium intermediate, **TS2**, with an overall barrier of 21.3 kcal.mol^{-1}. However, this is not

the step where the stereochemistry of the process is decided, as both products could be reached from here. The stereochemistry-determining step is the formation of the bicyclic iminium intermediate, where the C-C bond is formed, closing the product bicycle. This happens in **TS4**. It is important to notice that in this mechanism the benzoic acid co-catalyst affects the reaction rate (it is present in **TS2**), but not the stereoselectivity (it is absent in **TS4**). These results agree with experimental observations that changes in the nature of the acid affect the reaction rate, but not the enantiomeric excess. For the sake of completeness, we studied the full reaction mechanism without the co-catalyst, and the results are summarized in the Supporting Information. The preferred mechanism goes through formation of the same type of intermediates although barriers are higher. The rate-limiting step without the acid co-catalyst is the formation of enamine with a barrier of 29.2 kcal.mol^{-1}.

Computational Study on the Enantioselectivity: In the postulated mechanism presented above in Figure 2, the stereoselectivity-determining step of the whole process is the formation of the bicyclic iminium intermediate. The corresponding transition state, where a C-C bond forms has two main isomers: **TS4anti/re** and the **TS4syn/si**. Each of them has many conformations, only those lower in energy contribute in the enantioselectivity. To find them, we screened a very large number of conformers with the MM3 force field[25] as implemented in Macromodel 8.5[26] and we reevaluated the best conformers at the DFT level (Gaussian 09).[27] We have previously evaluated this methodology.[28] The preferred conformers show the rings of the bicycle in chair conformation, and the C=C bond attacks the carbonyl group of dione to form the six-membered chair ring. The structures also show two hydrogen bonds between a carbonylic oxygen of the dione and two NH bonds of the prolinamide. **TS4anti/re** is 4.5 kcal.mol^{-1} more stable than **TS4syn/si** which favors the anti/re structure with almost 100% enantiomeric excess (ee). The identity of the major product is correct, but our computed ee value overestimates the expected energy difference. We thus refined our computational method by introducing full dispersion effects in the geometry optimization. We re-optimized the lowest energy conformers of **TS4anti/re** and **TS4syn/si** with a method including Grimme's dispersion correction DFT-D2, namely B97D.[29] We also introduced corrections for basis set superposition error (BSSE).[30] With this improved method there are four transition states that must be taken into account, as there are two low energy conformers for each transition state. The relative energy of the different TSs is: 0.0, 0.4, 2.5 and 3.2 kcal.mol^{-1}, for **TS4anti/reA**, **TS4anti/reB**, **TS4syn/siA** and **TS4syn/siB** respectively. Considering again these four TSs leads to an ee value of 97.9%, very consistent with the experiment result (97% ee).[22c] The main difference between the **TS4anti/reA** and **TS4anti/reB** is in the relative orientation of SO_2R group. The same difference is observed between **TS4syn/siA** and **TS4syn/siB** (see Figure 3). The better description of the system with this methodology is expected to be mainly due to inclusion of DFT-D2 which results in a better description of weak interactions between substrate and catalyst.

Figure 3. Geometries and relative energies of **TS4anti/reA**, **TS4anti/reB**, **TS4syn/siA** and **TS4syn/siB**. Energies correspond to relative free energies in kcal.mol^{-1} with respect to separate reactants.

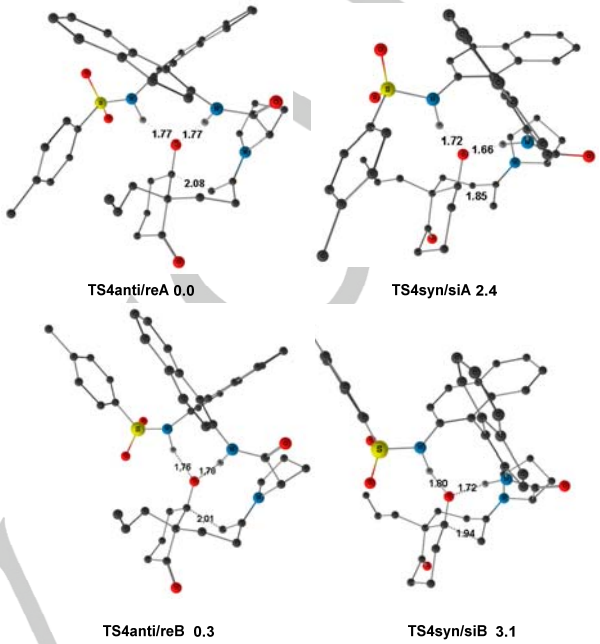

Once we reproduce the experimental result in terms of enantiomeric excess, we can analyze its origin. From examination of the geometries of **TS4anti/reA**, **TS4anti/reB**, **TS4syn/siA** and **TS4syn/siB** (Figure 3) the origin of the enantioselectivity is not clear. Hydrogen bonds play an important role, as they are rather strong, but there is not a clear pattern between the O...H distances and the stability of the transition states. Moreover, there is no obvious non-bonding interaction, either repulsive or attractive, between substrate and catalyst that explain in a simple way the discrimination between the diastereomeric transition states. We have performed an NCI plot[31] of two of the transition states, see computational details. This type of plots is useful to analyze the non-covalent interactions within the system under study.[21,32] In Figure 4, the NCI plots of **TS4anti/reB** and **TS4syn/siB** are presented, we can observe similar interactions in both TSs.

To obtain more insight, we carried out the energy decomposition analysis outlined in the thermodynamic cycle in Figure 5, which is based on the activation strain model.[33] The idea is to separate the system in two fragments, catalyst and substrate, and measure how distorted they are and how strongly they interact. The analysis is complicated by the presence of a double bond between the two fragments, which was sorted out by inclusion of the C=N bond in both fragments. Two hydrogens are also added and were optimized in the calculations, but the rest of the atoms were kept at the positions they have in the transition states. Distortion energies of fragments A and B can be easily evaluated through this procedure, however interaction energies cannot be evaluated independently due to the presence of the CH_2 groups. To sort that out we did not evaluate ΔE_{INT}, but $\Delta E_{INT(syn)} - \Delta E_{INT(anti)}$ instead, this energy can be easily achieved by completing the

thermodynamic cycle presented in Figure 5. Please note that in this case energies correspond to potential energies in solution. For the sake of simplicity, we will only compare one pair of isomers.

Figure 4. NCI plots of **TS4anti/reB** (left) and **TS4syn/siB** (right). Strong attractive interactions are represented in blue, week interactions in green and strong repulsive interactions in red.

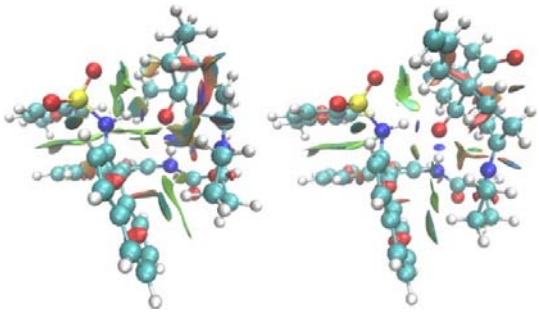

Figure 5. Energy decomposition diagram used in this study. Schematic structures and definition of the relative potential energies: ΔE relative potential energy between the two TSs, ΔE_{INT} interaction potential energy between the two fragments A and B in **TS4anti/re** and **TS4syn/si** and ΔE_{DIST} distortion energy of fragments A and B.

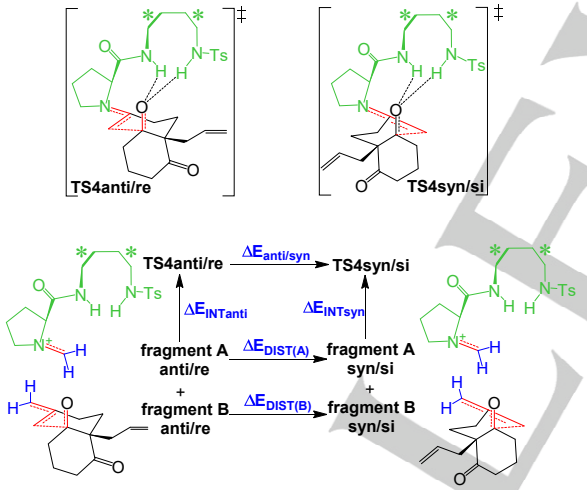

The prolinamide fragment (A) shows almost no differences in the two TSs, ΔE_{DIST} = 0.5 kcal.mol^{-1}. The substrate fragment (B) shows a larger energy difference, ΔE_{DIST} = 2.9 kcal.mol^{-1}. Completing the thermodynamic cycle, we obtain a value for interaction energies $\Delta E_{INT(syn)}$ - $\Delta E_{INT(anti)}$ = 1.0 kcal.mol^{-1}. This result is remarkable as it is contrary to the most usual case in enantioselective catalysis. In this system direct interactions between substrate and catalyst are not the leading term. The key is in the distortion terms, which are larger in the substrate fragment (B) than in the prolinamide catalyst (A). The catalyst is practically rigid. This is consistent with the known structural features of the binaphtyl group. The substrate (B) with its two fused six-membered rings is more flexible and distorts to obtain a better interaction with the catalyst. There are two regions of contact between catalyst and substrate. The first of them is the C=N double bond, and the second are the two hydrogen bonds between the acidic N-H groups in the catalyst and the oxygen developing a negative charge in the substrate. In the rigid structure of the catalyst, both interactions are pointing to precise regions in the space, and the substrate distorts to perform these interactions. This distortion is smaller in the case of anti/re, and this is why it leads to the major product.

The origin of enantioselectivity in this particular system is therefore not in the interaction of a particular region of the catalyst with a particular region of the substrate, but in the rigidity of the catalyst. This rigidity of the catalyst favors a certain arrangement of the substrate that leads to the major product.

Computational Study on Changes in the Catalyst. The impact of the catalyst substituents on the enantioselectivity was also computationally analyzed. As seen above it has been experimentally observed that changes on the R groups of the prolinamide have an effect on the experimental ee. These experiments were performed using the substrate 2-(2-oxopropyl)-2-methyl-cyclohexane-1,3-dione, **2** (R= Me), instead of the substrate **S** used in the mechanistic study (an allyl group is replaced by a methyl). The key transition states were recomputed for this substrate (**2** (R= Me)) and the different modified catalysts. The resulting computational ee values for each modified catalyst are presented in Table 3. Our computational results overestimate the observed ee but they are able to reproduce the experimentally observed trends (the energy order).

Table 3. Computational and experimental enantiomeric excess and relative energies for selected catalysts, which bear different substitution on R, see Figure 1. The relative free energies are for the different isomers of **TS4** respect to the most stable, in kcal.mol^{-1}.

	4	**5**	**7**	**8**	**9**	**10**
TS4anti/reA	0.0	0.0	0.0	0.0	1.9	0.0
TS4anti/reB	0.7	0.6		2.3	0.0	
TS4syn/siA	3.6	4.6	2.9	2.6	4.3	2.7
TS4syn/siB	4.3	3.5		3.6	4.7	
Computed ee	100%	100%	99%	98%	100%	42%
Experimental ee	94%	94%	86%	81%	90%	36%

Energy decomposition analysis was carried out for selected catalysts shown in Figure 1 (**4**, **5**, **7**, **8**, **9** and **10**) to investigate if the origin of enantioselectivity was similar. The results of the energy decomposition analysis are presented in Table 4. Not all systems behave in the same way. Catalysts **4**, **5**, **7** and **9** show the same trends we have seen for catalyst **3** with substrate **S**: the distortion energy of the substrate (B) is larger than the other terms and the distortion energy of the prolinamide catalyst (A) is small. Therefore, the catalyst is rigid and the differences in enantioselectivity for these four systems comes from the differences in the distortion of the substrate fragment (B). All these

four catalysts follow the same pattern in terms of rigidity, although there are also other effects that take place (**5** bears a bulky naphtyl substituent and **4** has an electron-withdrawing nitro group favoring stronger hydrogen bonds). In contrast, catalysts **8** and **10** follow a different pattern. For these two catalysts the most important term of the energy decomposition is the difference of interaction energies ($\Delta E_{INT(syn)}$-$\Delta E_{INT(anti)}$), so the origin of the enantioselectivity comes from the interaction between fragments. This is a more common situation in enantioselective catalysis. The distortion energies of these catalysts are negative (indicating preference for *syn* geometry) and in the case of catalyst **10** much larger, which means that the catalyst is less rigid. Analyzing in detail the geometries obtained for catalyst **10**, R= -$N(CH_3)_2$, we can see that the absence of the second N-H unit makes the structure more flexible, as there is no constraint associated with formation of N-H…X hydrogen bonds. The geometry of the **TS4anti/re** presents three hydrogen interactions on the C=O group of the dione, one with the NH bond and two with methyl groups of prolinamide. In contrast, in **TS4syn/si** the C=O group only interacts with a NH bond and a methyl group of prolinamide. **TS4anti/re** has thus more attractive interactions between fragments A and B than **TS4syn/si**. The case of **8** is subtler, the absence of the SO_2R group also giving more flexibility. It is therefore clear that the key to high enantioselectivity in these prolinamide systems is in the rigidity of the binam fragment, which should be maintained if one wants to keep selectivity. This is why systems **8** and **10** are steps in the wrong direction.

Table 4. Energy decomposition analysis for selected catalysts, which bear different substitution on R, see Figure 1. Relative potential energies in kcal.mol^{-1} between the different fragments prolinamide catalyst A and substrate B.

	4	**5**	**7**	**8**	**9**	**10**
$\Delta E_{DIST(A)}$	0.4	1.9	0.3	-0.8	0.6	-2.6
$\Delta E_{DIST(B)}$	3.5	3.6	2.8	0.9	3.7	-0.8
$\Delta E_{INT(syn)}$- $\Delta E_{INT(anti)}$	-0.5	-0.4	-0.6	3.0	-1.6	3.9
$\Delta E_{anty/syn}$	3.4	5.1	2.5	3.1	2.7	0.5

Conclusions

The intramolecular aldol reaction catalyzed by N-Ts(Sa)-binam-L-prolinamide leading to Wieland-Miescher ketones has been investigated experimentally and computationally. We have been able to clarify the mechanism of the reaction with prolinamide. It follows the general trends of the mechanism with proline, with the important caveat that the presence of a carboxylic acid as co-catalyst is mandatory in the initial steps of the reaction, in particular for the formation of the iminium intermediate. In contrast, the carboxylic acid has no effect on the enantioselectivity, as it departs the system after enamine formation, and is absent in the transition state leading to C-C bond formation. The origin of the enantioselectivity of the reaction has also been clarified. It is based on the rigidity of the catalyst, which has two anchoring points for the substrate, the C=N double bond in the enamine intermediate, and the N-H...O hydrogen bonds between catalyst and substrate. The substrate has to distort to bind properly to these anchoring points, and this distortion is smaller for the transition state leading to the favored enantiomer (anti/re). Changes in the structure of the catalyst were also experimentally and computationally investigated, and the resulting modifications in enantioselectivity were mainly due to changes in catalyst rigidity.

Experimental Section

Experimental details: General procedure for synthesis of Wieland-Miescher ketone 1 (using catalysts **3**-**10**) In a standard glass vial (10 × 3 cm) with stirrer bar was added triketone **2**[22c] (R = Me) followed by the corresponding catalyst and the acid. The resulting mixture darkened and was stirred for the indicated time. The mixture was absorbed onto silica and purified by column chromatography (0→5→10→25% EtOAc/ hexane) to give the Wieland-Miescher ketone (**1**) as a clear oil which solidified on standing to give a beige crystalline solid. HPLC (Daicel Chiralpak IC, Hexane/i-PrOH 80:20, 1 mL min-1, l = 254 nm; minor isomer t = 33.7 min, major isomer 37.8 min).

Computational details: Different methodologies have been used in the computational study. The initial mechanistic study started with optimization of minima and transition states with the B3LYP[34] functional as implemented in Gaussian 09[27] The 6-31g(d)[35] basis set was used for all atoms. Frequency calculations were carried out at the same level to confirm the nature of each stationary point and to obtain the free energies. Conformational searches were carried out for each minimum and transition state. Searches were performed with the Monte Carlo Multiple Minimum (MCMM)[36] searching methods and the MM3 force field[25] using the Macro Model program.[26] For each species the 10 lowest isomers were reoptimized at B3LYP level. Single point calculations with the M06-2X[37] functional and the 6-31+g(d,p) basis sets were then carried out with the ultrafine grid. Energies presented in the mechanistic part of the text correspond thus to M06-2X free energies in solution as single points on B3LYP optimized geometries. Solvent effects were taken into account by using the SMD[38] solvation model and approximating the experimental solvent (the substrate, **S**) to cyclohexanone. In the enantioselectivy study a more refined treatment was necessary to improve agreement with experiment. The **TS4** transition states were reoptimized using B97D[29] functional and the 6-31G(d) basis sets, then performed a single point with a larger basis set B97D/6-31+G(d,p). We evaluated and corrected the free energies by the basis set superposition error (BSSE).[30] Solvation was taken into account again with the SMD method as above. Plots of Non-covalent Interactions (NCI) were performed with promolecular densities and performed with NCIplot-3.0.[31] Interactions were represented following the recommendations in its manual (isovalue= 0.3). The geometries of all species relevant for this study are included in a data set collection of computational results available in the ioChem-BD repository.[39]

Acknowledgements

We thank for financial support the CERCA Programme /Generalitat the Catalunya and MINECO (project CTQ2017-87792-R and CTQ2016-75350-P). C.L. thanks the National Natural Science Foundation of China (No.21703195)

Conflict of Interest

The authors declare no conflict of interest

Keywords: organocatalysis · *N*-sulfonyl-binamprolinamide · asymmetric catalysis · DFT calculations · ketone

[1] Z. G. Hajos, D. R. Parrish, *J. Org. Chem.* **1974**, *39*, 1615-1621.
[2] U. Eder, G. Sauer, R. Wiechert, *Angew. Chem. Int. Ed.* **1971**, *10*, 496-497.
[3] B. Bradshaw, J. Bonjoch, *Synlett.* **2012**, *23*, 337-356.
[4] a) M. Agirre, A. Arrieta, I. Arrastia, F. P. Cossio, *Chem. Asian J.* **2019**, *14*, 44-66. b) I. Atodiresei, C. Vila, M. Rueping, *ACS Catal.* **2015**, *5*, 1972-1985. c) V. d. G. Oliveira, M. F. do Carmo Cardoso, L. d. S. Magalhaes Forezi, *Catalysts* **2018**, *8,* 605-624. d) C. Rodriguez-Escrich, M. A. Pericas, *Chem. Rec.* **2018**, *18*, 1-20. e) B. M. Trost, C. S. Brindle, *Chem. Soc. Rev.* **2010**, *39*, 1600-1632.
[5] a) P. Zhou, L. Zhang, S. Luo, J.-P. Cheng, J. Org. Chem. 2012, 88,2526-2530; b) S. Cañellas, C. Ayats, A. H. Henseler, M. A. Pericàs, *ACS Catal.* **2017**, *7*, 1383-1391.
[6] O. H. Rubio, Á. L. Fuentes de Arriba, L. M. Monleón, F. Sanz, L. Simón, V. Alcázar, J. R. Morán, Tetrahedron, **2015**, *71*, 1297-1303.
[7] a) C. F. I. Barbas, *Angew. Chem. Int. Ed.* **2008**, *47*, 42-47. b) N. Utsumi, M. Imai, F. Tanaka, S. S. V. Ramasastry, C. F. Barbas, III, *Org. Lett.* **2007**, *9*, 3445-3448.
[8] a) P. H.-Y. Cheong, C. Y. Legault, J. M. Um, N. Celebi-Oelcuem, K. N. Houk, *Chem. Rev.* **2011**, *111*, 5042-5137. b) M. Nielsen, D. Worgull, T. Zweifel, B. Gschwend, S. Bertelsen, K. A. Jorgensen, *Chem. Commun.* **2011**, *47*, 632-649. c) P. Renzi, J. Hioe, R. M. Gschwind, *Acc. Chem. Res.* **2017**, *50*, 2936-2948.
[9] C. Agami, F. Meynier, C. Puchot, J. Guilhem, C. Pascard, *Tetrahedron* **1984**, *40*, 1031-1038.
[10] K. Sakthivel, W. Notz, T. Bui, C. F. Barbas, *J. Am. Chem. Soc.* **2001**, *123*, 5260-5267.
[11] L. Hoang, S. Bahmanyar, K. N. Houk, B. List, *J. Am. Chem. Soc.* **2003**, *125*, 16-17.
[12] a) S. Bahmanyar, K. N. Houk, *J. Am. Chem. Soc.* **2001**, *123*, 12911-12912. b) S. Bahmanyar, K. N. Houk, *J. Am. Chem. Soc.* **2001**, *123*, 11273-11283.
[13] B. List, R. A. Lerner, C. F. Barbas, *J. Am. Chem. Soc.* **2000**, *122*, 2395-2396.
[14] D. Seebach, A. K. Beck, D. M. Badine, M. Limbach, A. Eschenmoser, A. M. Treasurywala, R. Hobi, W. Prikoszovich, B. Linder, *Helv. Chim. Acta* **2007**, *90*, 425-471.
[15] H. Iwamura, D. H. Wells, S. P. Mathew, M. Klussmann, A. Armstrong, D. G. Blackmond, *J. Am. Chem. Soc.* **2004**, *126*, 16312-16313.
[16] B. List, L. Hoang, H. J. Martin, *Proc. Natl. Acad. Sci. U.S.A.*, **2004**, *101*, 5839 -5842.
[17] a) M. H. Haindl, J. Hioe, R. M. Gschwind, *J. Am. Chem. Soc.* **2015**, *137*, 12835-12842. b) A. K. Sharma, R. B. Sunoj, *Angew. Chem. Int. Ed.* **2010**, *49*, 6373-6377.
[18] a) C. T. Wong, *Tetrahedron Lett.* **2009**, *50*, 811-813. b) T. Kanzian, S. Lakhdar, H. Mayr, *Angew. Chem. Int. Ed.* **2010**, *49*, 9526-9529.
[19] M. B. Schmid, K. Zeitler, R. M. Gschwind, *Angew. Chem. Int. Ed.* **2010**, *49*, 4997-5003.
[20] a) A. Fu, C. Tian, H. Li, P. Li, T. Chu, Z. Wang, J. Liu, *Chem. Phys.* **2015**, *455*, 65-72. b) A. K. Sharma, R. B. Sunoj, *J. Org. Chem.* **2012**, *77*, 10516-10524. c) U. I. Tafida, A. Uzairu, S. E. Abechi, *J. Adv. Res.* **2018**, *12*, 11-19.
[21] C. Liu, M. Besora, F. Maseras, *Chem. Asian J.* **2016**, *11*, 411-416.
[22] a) B. Bradshaw, G. Etxebarria-Jardí, J. Bonjoch, *J. Am. Chem. Soc.* **2010**, *132*, 5966-5967. b) B. Bradshaw, G. Etxebarria-Jardí, J. Bonjoch, S. Viózquez, G. Guillena, C. Nájera, *Org. Synth*. **2011**, *88*, 330-341. c) B. Bradshaw, G. Etxebarría-Jardi, J. Bonjoch, S. F. Viózquez, G. Guillena, C. Nájera, *Adv. Synth. Catal.* **2009**, *351*, 2482-2490. d) S. F. Viózquez, G. Guillena, C. Nájera, B. Bradshaw, G. Etxebarria-Jardí, J. Bonjoch, *Org. Synth.* **2011**, *88*, 317-329.
[23] J.-S. Oh, J. W. Lee, T. H. Ryu, J. H. Lee, C. E. Song, *Org. Biomol. Chem.,* **2012**, *10*, 1052-1055 and references cited therein.
[24] B. Bradshaw, G. Etxebarría-Jardi, J. Bonjoch, S. Viózquez, G. Guillena, C. Nájera, *Org. Synth*., **2011**, *88*, 330-341.
[25] N. L. Allinger, Y. H. Yuh, J. H. Lii, *J. Am. Chem. Soc.* **1989**, *111*, 8551-8566.
[26] F. Mohamadi, N. G. J. Richards, W. C. Guida, R. Liskamp, M. Lipton, C. Caufield, G. Chang, T. Hendrickson, W. C. Still, *J. Comput. Chem.* **1990**, *11*, 440-467.
[27] M. J. T. Frisch, G. W.; Schlegel, H. B.; Scuseria, G. E.; Robb, M. A.; Cheeseman, J. R.; Scalmani, G.; Barone, V.; Mennucci, B.; Petersson, G. A.; Nakatsuji, H.; Caricato, M.; Li, X.; Hratchian, H. P.; Izmaylov, A. F.; Bloino, J.; Zheng, G.; Sonnenberg, J. L.; Hada, M.; Ehara, M.; Toyota, K.; Fukuda, R.; Hasegawa, J.; Ishida, M.; Nakajima, T.; Honda, Y.; Kitao, O.; Nakai, H.; Vreven, T.; Montgomery, J. A., Jr.; Peralta, J. E.; Ogliaro, F.; Bearpark, M.; Heyd, J. J.; Brothers, E.; Kudin, K. N.; Staroverov, V. N.; Kobayashi, R.; Normand, J.; Raghavachari, K.; Rendell, A.; Burant, J. C.; Iyengar, S. S.; Tomasi, J.; Cossi, M.; Rega, N.; Millam, J. M.; Klene, M.; Knox, J. E.; Cross, J. B.; Bakken, V.; Adamo, C.; Jaramillo, J.; Gomperts, R.; Stratmann, R. E.; Yazyev, O.; Austin, A. J.; Cammi, R.; Pomelli, C.; Ochterski, J. W.; Martin, R. L.; Morokuma, K.; Zakrzewski, V. G.; Voth, G. A.; Salvador, P.; Dannenberg, J. J.; Dapprich, S.; Daniels, A. D.; Farkas, Ö.; Foresman, J. B.; Ortiz, J. V.; Cioslowski, J.; Fox, D. J., *Vol. RevisionD.01*, Gaussian, Inc., Wallingford CT, 2009.
[28] M. Besora, A. A. C. Braga, G. Ujaque, F. Maseras, A. Lledós, *Theor. Chem. Acc.* **2011**, *128*, 639-646.
[29] S. Grimme, *J. Comput. Chem.* **2006**, *27*, 1787-1799.
[30] R. M. Balabin, *J. Chem. Phys.* **2008**, *129*, 164101-164105.
[31] a) E. R. Johnson, S. Keinan, P. Mori-Sánchez, J. Contreras-García, A. J. Cohen, W. Yang, *J. Am. Chem. Soc.* **2010**, *132*, 6498-6506. b) J. Contreras-García, E. R. Johnson, S. Keinan, R. Chaudret, J.-P. Piquemal, D. N. Beratan, W. Yang, *J. Chem. Theory Comput.* **2011**, *7*, 625-632.
[32] a) X. Li, D. Wei, Z. Li, *ACS Omega* **2017**, *2*, 7029-7038. b) Y. Wang, Y. Wang, X. Wang, X. Li, L.B. Qu D. Wei, *Catal. Sci. Technol.*, **2018**, *8*, 4229-4240. c) X. Li, Y. Wang, Y. Wang, M. Tang, L.B. Qu, Z. Li, and D. Wei, *J. Org. Chem.* **2018**, *83*, 8543-8555.
[33] a) I. Fernández, F. M. Bickelhaupt, *Chem. Soc. Rev*. **2014**, *43*, 4953-4967. b) F. M. Bickelhaupt, K. N. Houk, *Angew. Chem. Int. Ed.* **2017**, *56*, 10070-10086.
[34] a) A. D. Becke, *J. Chem. Phys.* **1993**, *98*, 5648-5652. b) P. J. Stephens, F. J. Devlin, C. F. Chabalowski, M. J. Frisch, *J. Phys. Chem.* **1994**, *98*, 11623-11627. c) C. Lee, W. Yang, R. G. Parr, *Phys. Rev. B* **1988**, *37*, 785-789.
[35] a) R. Ditchfield, W. J. Hehre, J. A. Pople, *J. Chem. Phys.* **1971**, *54*, 724-728. b) W. J. Hehre, R. Ditchfield, J. A. Pople, *J. Chem. Phys.* **1972**, *56*, 2257-2261. c) P. C. Hariharan, J. A. Pople, *Theor Chim Acta* **1973**, *28*, 213-222.
[36] a) G. Chang, W. C. Guida, W. C. Still, *J. Am. Chem. Soc.* **1989**, *111*, 4379-4386. b) M. Saunders, K. N. Houk, Y. D. Wu, W. C. Still, M. Lipton, G. Chang, W. C. Guida, *J. Am. Chem. Soc.* **1990**, *112*, 1419-1427.
[37] Y. Zhao, D. G. Truhlar, *Theor. Chem. Acc.* **2008**, *120*, 215-241.
[38] A. V. Marenich, C. J. Cramer, D. G. Truhlar, *J. Phys. Chem. B* **2009**, *113*, 6378-6396.
[39] M. Álvarez-Moreno, C. de Graaf, N. López, F. Maseras, J. M. Poblet, C. Bo, *J. Chem. Inf. Model.* **2015**, *55*, 95-103.

Entry for the Table of Contents (Please choose one layout)

Layout 1:

FULL PAPER

Rigidity is key for enantioselectivity. The high enantioselectivity in the synthesis of the Wieland-Miescher ketone (WMK) catalyzed by *N*-sulfonyl-binamprolinamides is shown to be based on the rigidity of the organoccatalyst, a result which is confirmed by the behavior of modified versions of the molecule.

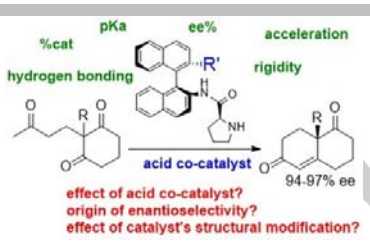

Chunhui Liu, Ben Bradshaw, Feliu Maseras, Josep Bonjoch, Maria Besora**

Page No. – Page No.

Mechanistic study on the asymmetric synthesis of the Wieland-Miescher ketone and analogues.